

## Precision measurements of the electron spectrum and the positron spectrum with AMS

S. SCHAEEL<sup>1</sup> FOR THE AMS COLLABORATION<sup>2</sup>.

<sup>1</sup> *I. Physikalisches Institut B, RWTH Aachen University, 52074 Aachen, Germany*

<sup>2</sup> *for the complete list of authors see the AMS-Collaboration list in these proceedings.*

*schael@physik.rwth-aachen.de*

**Abstract:** The AMS-02 detector is operational on the International Space Station since May 2011. More than 30 billion events have been collected. Recently, results on the positron fraction have been published [1]. Further investigation of cosmic-ray electrons and positrons must hinge on the individual energy spectra of these species. Similar to the data analysis used to determine the positron fraction, the number of electron and positron events measured with AMS-02 are evaluated by an analysis method using template fits. In this contribution, we will review analysis techniques used to determine the individual fluxes of cosmic-ray electrons and positrons. The presented electron and positron fluxes are preliminary and represent work in progress. Systematic uncertainties must still be investigated further.

**Keywords:** AMS-02, cosmic-rays, flux, electrons, positrons.

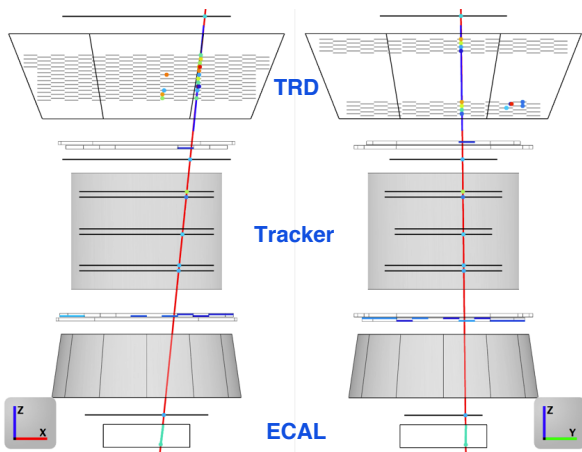


**Figure 1:** Event display of a 1.3 TeV electron passing through the AMS-02 detector.

### 1 Introduction

The AMS-02 experiment is a multi-purpose particle detector mounted on the International Space Station (ISS). It has been gathering data since May 2011 detecting and identifying cosmic-ray electrons, positrons, protons, anti-protons, nuclei up to iron, and photons. Recently, first results on the measurement of the cosmic-ray positron fraction have been published [1] and will be presented at this conference [2]. This measurement of unprecedented accuracy extends to 350 GeV and emphasizes the need of a primary source of positrons to explain the rise of the positron fraction at high energies.

Investigations of such a source must include a description of the individual fluxes of cosmic-ray electrons and positrons. The currently available measurements, especially of the positron flux, do not allow a detailed investigation of a common source. Especially for positrons, the latest published data, by HEAT in 2000 [3], reaches only up to 50 GeV in energy. Thus, a precise measurement of the

fluxes of electrons and positrons to high energies is an important cornerstone of the science program for AMS-02. In this contribution we report progress towards these measurements, for positrons up to 350 GeV and for electrons up to 500 GeV. Another contribution describes the analysis towards an inclusive energy spectrum of electrons and positrons [4].

### 2 The AMS-02 Detector

The AMS-02 detector consists of nine planes of precision silicon tracker [5] with 6 planes of the inner tracker inside the bore of a permanent magnet, a transition radiation detector (TRD, see also [6]), four planes of time of flight counters (TOF), an array of anti-coincidence counters (ACC) surrounding the inner tracker, a ring imaging Cherenkov detector (RICH) [7], and an electromagnetic calorimeter (ECAL, see also [8, 9]). For a detailed detector description see [1]. An electron event with measured energy of 1.3 TeV is shown in Figure 1.

There are three main detectors that allow a significant reduction of the tremendous proton background in the identification of the positron and electron samples. These are the TRD, the ECAL, and the tracker. In order to differentiate in the TRD between  $e^\pm$  and protons, up to 20 signals from the TRD layers are combined in a TRD estimator formed from the ratio of the log-likelihood probability of the  $e^\pm$  hypothesis to that of the proton hypothesis. The probabilities are calculated from the probability density functions  $f(s)$  of the TRD signals  $s$  for each species hypothesis as, e.g.  $P_{e^\pm} = \frac{f_{e^\pm}(s)}{\sum_i f_{e^\pm}(s_i)}$ . The proton rejection power of the TRD estimator at 90% efficiency for  $e^\pm$  measured on orbit is  $10^3$  to  $10^4$  [1]. The proton rejection power of the ECAL estimator (determined by a boosted decision tree algorithm) when combined with a matching of energy and momentum measured in the tracker reaches  $\sim 10^4$  [1]. Note that the proton rejection power can be readily improved by tightening the selection criteria with reduced  $e^\pm$  efficiency.

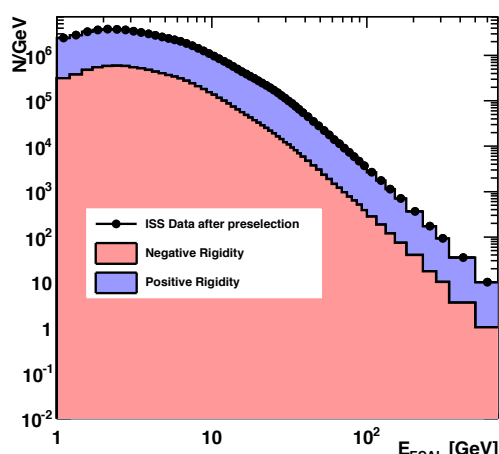


**Figure 2:** Raw energy spectra of events passing all quality criteria for this analysis. Positively and negatively charged events are shown in comparison.

### 3 Data Analysis

The flux of cosmic-ray electrons or positrons  $\phi_{e^\pm}$  in energy bins  $\Delta E$  can be determined as

$$\phi_{e^\pm} = \frac{N_{e^\pm}}{A_{eff.} \cdot \epsilon_{trig} \cdot \epsilon_{sel} \cdot T \cdot \Delta E}, \quad (1)$$

with the number of measured electrons or positrons  $N_{e^\pm}$ , the effective acceptance  $A_{eff.}$ , trigger efficiency  $\epsilon_{trig}$ , selection efficiency  $\epsilon_{sel}$ , and measurement time  $T$ .

The width  $\Delta E$  of the energy bins are chosen sufficiently large with respect to the energy resolution of the ECAL. This minimizes necessary corrections to the fluxes by unfolding. At high energies still larger bin sizes ensure sufficient counting statistics in each bin.

The event numbers  $N_{e^\pm}$  in each bin are evaluated following a similar procedure as described in [1]. A loose preselection is used to define measurement times of stable detector operations for the whole data set. Further quality cuts define a high quality data set with excellent and unambiguous event reconstruction: Events are selected by requiring a track in the TRD and in the tracker, a cluster of hits in the ECAL, and a measured velocity  $\beta > 0$  in the TOF consistent with a downward-going  $Z = 1$  particle. 30 million events pass this selection. Figure 2 shows the raw energy spectrum of these events. Above the energy scale of geomagnetic cutoff and solar modulation the raw spectrum is a straight power law, also for the distinct event classes with positive and negative reconstructed charge sign. In the energy range from 50 to 100 GeV, Figure 3 shows the ECAL and TRD estimators to separate four event classes that can be loosely identified as negative electron-like, positive electron-like, positive proton-like, and negative proton-like events.

In the following the ECAL estimator and  $E/R$  matching are used to further reject protons. The cuts are chosen to have a high efficiency, but still reduce the proton background significantly. The resulting event samples of electron and positron candidate events are then evaluated by template fits to the distribution of the TRD estimator. By varying the normalizations of signal and background templates, the template fits for positive and negative rigidities

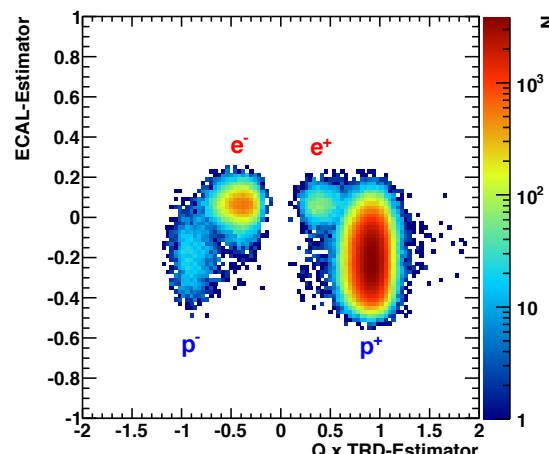


**Figure 3:** All events after preselection ( $Z = 1$ ) cluster in four areas in a correlation of the ECAL and TRD estimators. Positive and negative electron and proton like events are clearly distinct.

determine the total number of positrons and electrons, respectively, in any given energy bin. In this way the analysis utilizes the identification power of the three estimators and determines efficiently the number of electrons and positrons. An example of these fits is shown in Figure 4 for the energy bin from 132 to 152 GeV. The reduced  $\chi^2$  of all fits indicate a good fit quality for all energy bins. Clearly, two components can be identified in the distributions for electrons and positrons. A small background of proton-like events needs to be subtracted from the electron-like events after ECAL cuts. The positron-like events suffer from a significant background of protons that can be readily taken into account by the fit. The signal and background templates needed for this analysis can be generated from data or simulation, but must be determined for every energy bin as the TRD estimator is energy dependent. Templates from data are determined for protons by reversing the ECAL estimator and  $E/R$  matching cuts. For this procedure, a large data set is needed and therefore this is a viable approach to define template distributions for proton events. The distribution of the TRD estimator can also be generated by Monte Carlo (see below) simulation, which yields statistically accurate templates. Especially for electron events, for which the energy dependence of the TRD estimator is minute, this approach is preferred. Both types of templates, determined from data or simulation, agree very well and yield comparable results in the fits.

The effect of charge confusion must be carefully investigated. At high energies a fraction of negatively charged events (electrons) is reconstructed as positively charged events (positrons), and vice versa. The amount of charge confusion has been studied in data and simulation. Both studies agree, as described in [1], and indicate a charge confusion of about 3% at 300 GeV. For this analysis the result of the Monte Carlo simulation is used to correct the electron and positron spectra.

The trigger efficiency  $\epsilon_{trig}$  is determined from data. In addition to physics triggered events, AMS records so-called unbiased triggers (with a scaling factor of  $f_{PS}$ ). The trigger efficiency is then given by

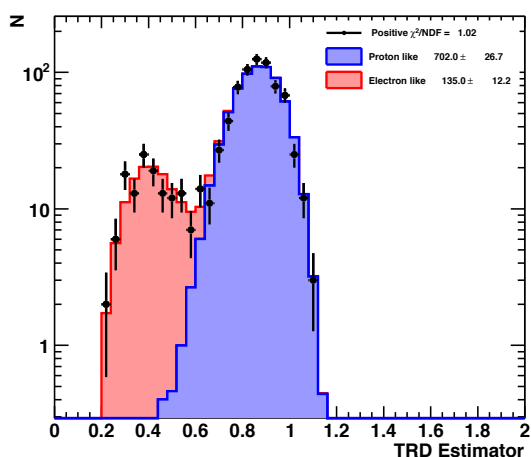
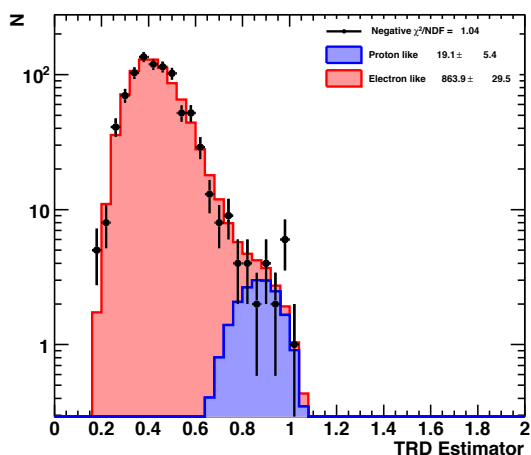


**Figure 4:** Template fits to the TRD estimator for negatively charged (top) and positively charged (bottom) events between 132 to 152 GeV. The number of electron like and proton events can be clearly identified.

$$\epsilon_{trig} = N_{phys} / (N_{phys} + f_{PS} \cdot N_{ubias}).$$

In Figure 5 the resulting trigger efficiency is shown as a function of energy.

Above an energy of 3 GeV the trigger efficiency is constant and very close to unity. A full Geant 4 [10] Monte Carlo (MC) simulation of the complete AMS detector is used to determine the geometrical acceptance  $A$  and the efficiency of the pre-selection and quality selection cuts  $\epsilon_{sel}$ . The MC program simulates electromagnetic and hadronic interactions of particles in the materials of AMS and generates detector responses. The digitization of the signals, including those of the AMS trigger, is simulated precisely according to the measured characteristics of the electronics. The digitized signals then undergo the same reconstruction as used for the data. The acceptance of AMS-02 requiring passage through the TRD, electromagnetic calorimeter, and trigger (TOF) is determined to be about 950 cm<sup>2</sup> sr at an energy of 50 GeV. Figure 6 shows the effective acceptance, i.e. the geometrical acceptance modified by the pre-selection efficiency, as a function of MC-generated energy. It is found to be only slightly dependent on energy above 3 GeV. It should be noted that at high energies the acceptance is restricted to the full tracker geometry to ensure a reliable determination of

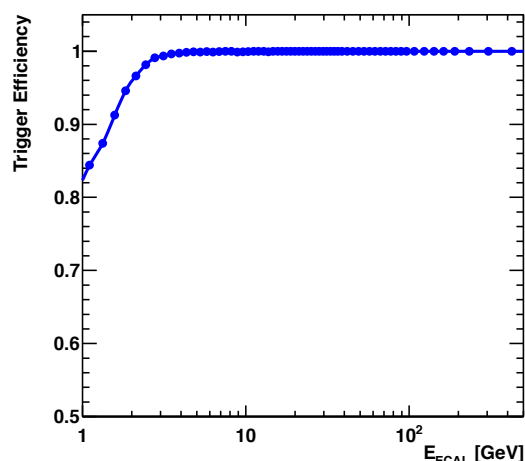


**Figure 5:** Trigger efficiency for electrons as a function of energy.

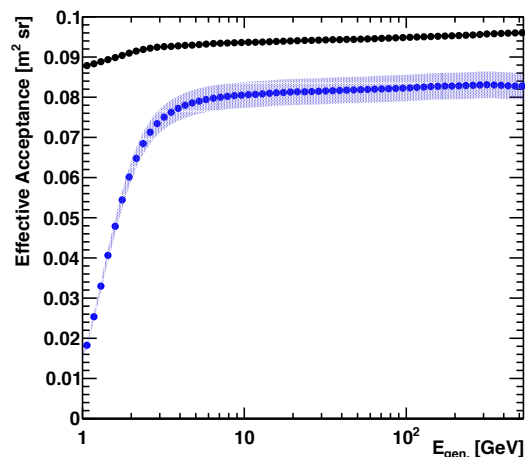


**Figure 6:** Acceptance of the AMS-02 detector (upper black line). Pre-selection reduces the effective acceptance (lower blue line). The band indicates the 4% systematic error.

the charge sign and therefore minimizes the effect of charge confusion. A 4% systematic uncertainty band is shown in Fig. 6, which is, however, still under investigation.

The AMS trigger rate is shown in Figure 7. We have analyzed data taken from 19 May 2011 to 11 March 2013. For each second, the global status of AMS is defined with several parameters. The exposure time period is selected as follows:

- AMS is in the nominal data taking status,
- AMS vertical axis is within 25° of the Earth zenith axis, and
- the measured ECAL energy is required to exceed by a factor 1.2 the maximal Stoermer cutoff [11].

The total exposure time depends on the measured ECAL energy and is for energies above 30 GeV constant at 4.38 · 10<sup>7</sup> seconds, which corresponds to an overall average live time fraction of 80.2% for this time interval.

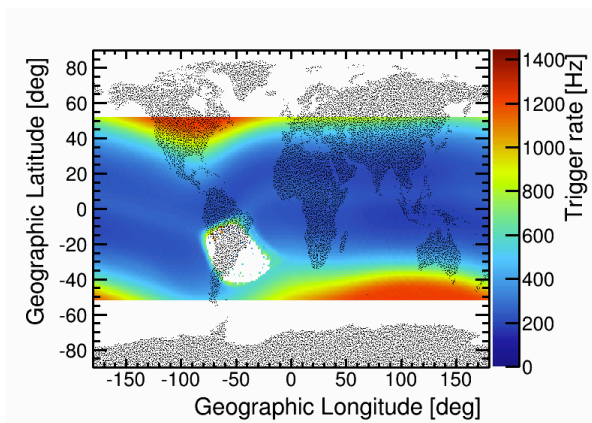


**Figure 7:** Trigger rate as a function of orbital position. Variations are correlated with the geomagnetic cutoff rigidity.

## 4 Results

All information can now be used to calculate the energy spectra for electrons and positrons according to Eq. (1). These preliminary fluxes multiplied by the third power of the energy are shown in Figure 8.

The electron flux measurement extends up to 500 GeV. Multiplied by  $E^3$  it is rising up to 10 GeV and appears to be on a smooth, slowly falling curve above. The measurement is in good agreement with the previous data reported by the PAMELA experiment [12] and HEAT experiment [3]. The differences at low energies can be attributed to the effect of solar modulation.

The positron flux measurement extends up to 350 GeV. Multiplied by  $E^3$  it is rising up to 10 GeV, from 10 to 30 GeV the spectrum is flat and above 30 GeV again rising as indicated by the black line in the figure. The spectral index and its dependence on energy is clearly different from the electron spectrum. In the low energy range the agreement with results reported by the HEAT experiment [3] is good.

## 5 Conclusions

Data record by the AMS experiment in the time interval from 19 May 2011 to 11 March 2013 have been analyzed. This corresponds only to 10% of the expected total data volume. Combining the particle identification power of the high precision silicon tracker, the 17 radiation lengths deep electromagnetic calorimeter, and the 20 layer transition radiation detector allows to clearly separate cosmic-ray electrons and positrons from the large proton background.

A first measurement of the electron flux up to 500 GeV and of the positron flux up to 350 GeV has been presented. Details of the systematic errors are still under investigation. The measured spectra show smooth curves with no particular fine structures. The positron spectrum shows a break at around 30 GeV energy. Differences in the spectral indices of electrons and positrons as expected from the positron fraction measurement [1] are clearly visible.

## 6 Acknowledgements

This work has been supported by persons and institutions acknowledged in [1], as well as by the Italian Space Agency under contracts ASI-INFN I/002/13/0 and ASDC/011/11/1.

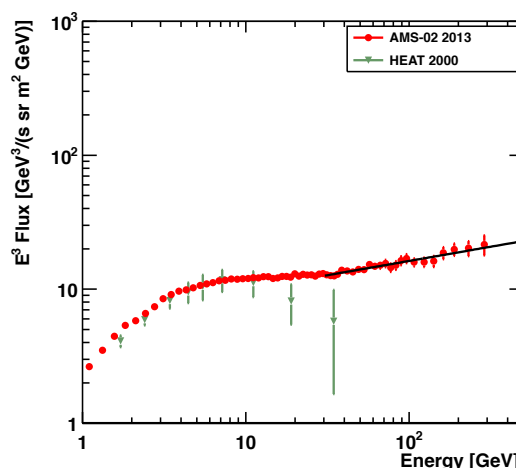
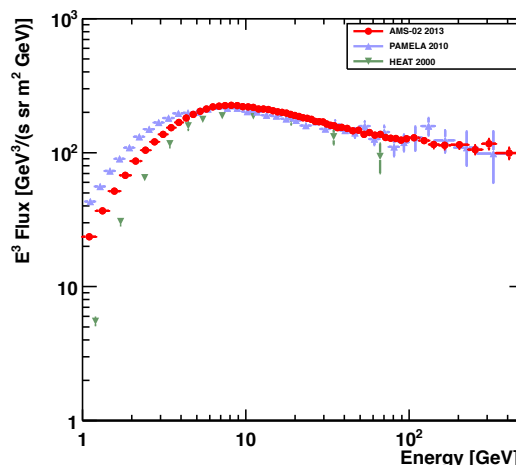


**Figure 8:** Electron (top) and positron (bottom) fluxes as measured by AMS-02. For comparison, data from PAMELA [12] and HEAT [3] are shown. Data points are positioned within the energy bins according to [13]

## References

- [1] M. Aguilar et al., Phys. Rev. Lett. 110 (2013) 141102 doi: 10.1103/PhysRevLett.110.141102.
- [2] A. Kounine, AMS collab., this conference (ID 1264)
- [3] M. A. DuVernois et al., ApJ 559 (2001) 296
- [4] B. Bertucci, AMS collab., this conference (ID 1267)
- [5] J. Bazo, AMS collab., this conference (ID 0849)
- [6] C. Delgado, AMS collab., this conference (ID 1260)
- [7] H. Gast, AMS collab., this conference (ID 0359)
- [8] M. Aguilar-Benitez et al., NIM A 614 (2010) 237
- [9] S. Di Falco, AMS collab., this conference (ID 0855)
- [10] C. Adloff et al., NIM A 714 (2013) 147
- [11] J. Allison et al., IEEE Trans. Nucl. Sci. 53 (2006) 270
- [12] C. Stoermer, The Polar Aurora (Oxford University, London, 1950)
- [13] O. Adriani et al., Phys. Rev. Lett. 106 (2011) 201101
- [14] G. D. Lafferty and T. R. Wyatt, NIM A 355 (1995) 541